Fibroblast growth factor signaling instructs ensheathing glia wrapping of *Drosophila* olfactory glomeruli

Bing Wu[a,b], Jiefu Li[a,b], Ya-Hui Chou[c], David Luginbuhl[a,b], and Liqun Luo[a,b,1]

[a]Howard Hughes Medical Institute, Stanford University, Stanford, CA 94305; [b]Department of Biology, Stanford University, Stanford, CA 94305; and [c]Institute of Cellular and Organismic Biology, Academia Sinica, Taipei 11529, Taiwan

This contribution is part of the special series of Inaugural Articles by members of the National Academy of Sciences elected in 2012.

Contributed by Liqun Luo, June 5, 2017 (sent for review April 19, 2017); reviewed by Marc Freeman and Tzumin Lee

The formation of complex but highly organized neural circuits requires interactions between neurons and glia. During the assembly of the *Drosophila* olfactory circuit, 50 olfactory receptor neuron (ORN) classes and 50 projection neuron (PN) classes form synaptic connections in 50 glomerular compartments in the antennal lobe, each of which represents a discrete olfactory information-processing channel. Each compartment is separated from the adjacent compartments by membranous processes from ensheathing glia. Here we show that Thisbe, an FGF released from olfactory neurons, particularly from local interneurons, instructs ensheathing glia to wrap each glomerulus. The Heartless FGF receptor acts cell-autonomously in ensheathing glia to regulate process extension so as to insulate each neuropil compartment. Overexpressing Thisbe in ORNs or PNs causes overwrapping of the glomeruli their axons or dendrites target. Failure to establish the FGF-dependent glia structure disrupts precise ORN axon targeting and discrete glomerular formation.

ensheathing glia | FGF | olfactory glomeruli | neuropil compartmentalization | ORN axon targeting

Glia and neurons interact dynamically to coordinate the development and function of neural circuits. For example, *Drosophila* midline glia serve as guideposts that provide spatial cues to direct axonal pathfinding in the embryonic ventral nerve cord (1, 2). Neurons in turn provide signals that weave glia into the fabric of the nervous system. For instance, axonal Neuregulin-1 levels dictate the extent of Schwann cell myelination (3). A myriad of other biological processes in the developing and adult brain, including synapse formation (4–7), elimination (8, 9), and regulation of synaptic activity (10–13), require extensive communication and cooperation between neurons and glia.

The *Drosophila* nervous system contains a diverse array of glial cell types (14), thus offering opportunities to discover new mechanisms for glia–neuron interactions. Ensheathing glia are groups of cells that insulate neighboring neuropil structures by extending their membranous processes along the outer surface of synaptic neuropils or their subcompartments without invading the inner part of the neuropil (15). It remains unknown how ensheathing glia establish such a barrier-like structure, what molecular signals orchestrate this process, and whether the glial barrier is essential for the integrity of the encircled neuropil.

The *Drosophila* antennal lobe provides an excellent experimental system for tackling these questions with high resolution. The antennal lobe is organized into 50 discrete neuropil compartments, the glomeruli, wherein specific types of olfactory receptor neuron (ORN) axons and projection neuron (PN) dendrites form synapses. Each glomerulus is surrounded by ensheathing glia processes (15–17). In addition, the specific and stereotypic pattern of neuronal projections in the antennal lobe (18, 19) renders the system convenient for exploring the potential neuronal disorganization caused by the malformation of glial structures. Previous studies have used this system to find that in adult *Drosophila* the ensheathing glia increase their process extension to injured axons (20), help clear degenerating axons (20), and strengthen excitatory interactions between surviving neurons (21). Here we study ensheathing glia in the antennal lobe formation and organization during development.

Results

Pupal Development of Antennal Lobe Ensheathing Glia. To study the development and function of antennal lobe ensheathing glia, we searched for genetic tools that can label these cells specifically during the pupal stage when the olfactory circuit in the antennal lobe is being assembled. We preselected a number of enhancer-GAL4 lines from the FlyLight GAL4 collection based on the published expression pattern in adult animals (22) and from a few *MiMIC-GAL4* lines (23). We tested whether these GAL4 lines were active at different pupal stages. We found that at 96 h after puparium formation (hAPF), a late stage in antennal lobe morphogenesis, *SPARC-GAL4* (Fig. 1*D*), *GMR56F03-GAL4* (Fig. S1) (24), and *GMR10E12-GAL4* (Fig. S1) flies expressed GAL4 predominantly in ensheathing glia. As indicated by the *UAS-mCD8GFP* reporter that labeled the cell membranes and processes in the presence of GAL4, these GAL4$^+$ cells were located on the periphery of the antennal lobe and extended their processes to wrap around the antennal lobe and around individual glomeruli within it but with minimal invasion into each glomerulus. These morphological features are characteristic of ensheathing glia. We also used *UAS-nuclear-LacZ* to mark the nuclei of these GAL4$^+$ cells (Fig.

Significance

This research reports that reciprocal interactions between *Drosophila* olfactory neurons and ensheathing glia mediate the formation of neuronal compartments, groups of synapses that are packed into discrete structures called "glomeruli" that carry specific olfactory information. Ensheathing glia respond to a neuronal cue, the FGF Thisbe, to pattern the boundaries of the nascent compartments. Neural compartments, in turn, require such glial barriers to separate themselves from neighboring compartments and thus ensure the correct organization of the olfactory circuit. These findings highlight the importance of glia in the assembly and maintenance of neural circuits and the functions of FGF signaling in these processes.

Author contributions: B.W. and L.L. designed research; B.W. and J.L. performed research; Y.-H.C. and D.L. contributed new reagents/analytic tools; B.W. analyzed data; and B.W. and L.L. wrote the paper.

Reviewers: M.F., Vollum Institute, Oregon Health and Science University; and T.L., Howard Hughes Medical Institute.

The authors declare no conflict of interest.

Freely available online through the PNAS open access option.

[1]To whom correspondence should be addressed. Email: lluo@stanford.edu.

This article contains supporting information online at www.pnas.org/lookup/suppl/doi:10.1073/pnas.1706533114/-/DCSupplemental.

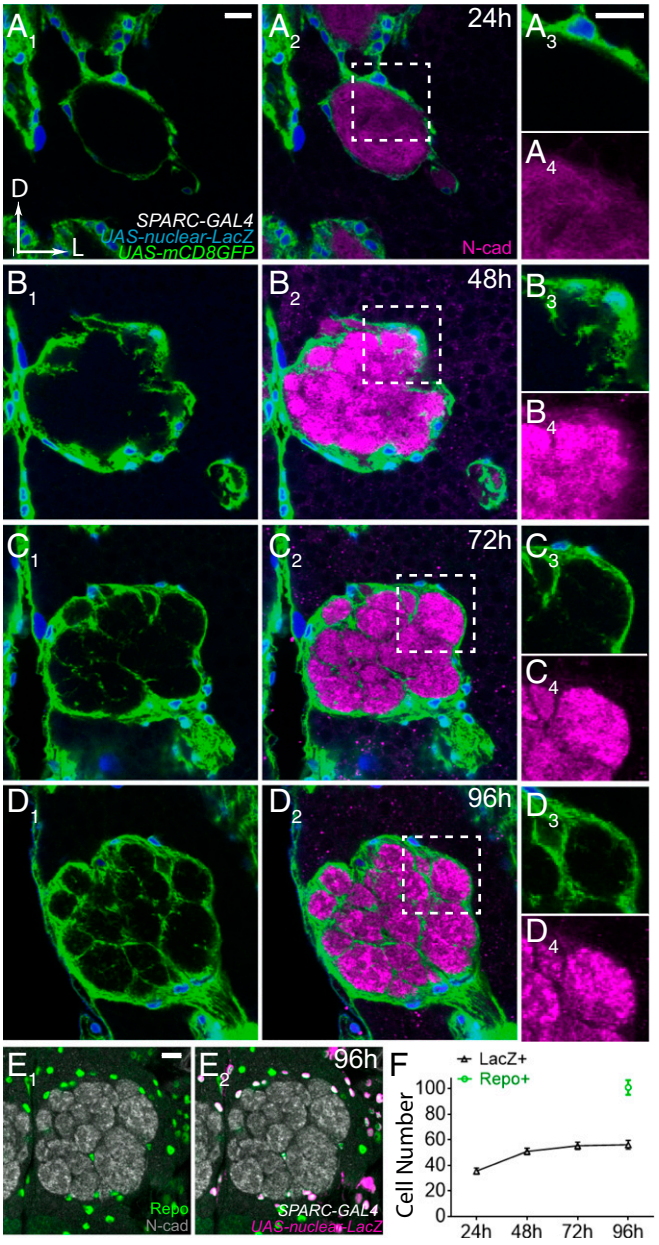

Fig. 1. Ensheathing glia morphogenesis during antennal lobe development. (*A–D*) Confocal sections of the antennal lobe at 24 (*A*), 48 (*B*), 72 (*C*), and 96 (*D*) hAPF. Ensheathing glia processes are labeled by *SPARC-GAL4*–driven (>) *UAS-mCD8GFP*. Ensheathing glia nuclei are marked by *UAS-nuclear-LacZ*. Neuropil staining by the Ncad antibody is shown as magenta. Dashed rectangles in center images are enlarged in the right column. D, dorsal; L, lateral. (Scale bars: 10 μm.) (*E*) Confocal sections of the antennal lobe at 96 hAPF. Glia nuclei stained by the Repo antibody are shown in green and are overlaid on the LacZ channel in E_2. (*F*) Quantification of the number of antennal lobe ensheathing glia cells at different developmental stages and the number of total glia around the antennal lobe at the end of pupae stage. Error bars represent SD. $n = 5$ for each time point. In this figure, subpanels represent the same sample in different imaging channels, unless otherwise specified.

1*E*) and found that every LacZ$^+$ nucleus around the antennal lobe (within 10 μm of the surface of the antennal lobe) was also positive for Repo, a glia marker in *Drosophila* (25), confirming that these GAL4$^+$ cells are indeed glia. On average, ~100 Repo$^+$ cells were detected around the antennal lobe, and ~56 of these were LacZ$^+$ (Fig. 1*F*). Repo$^+$/LacZ$^-$ cells are likely astrocytes and cortex glia present in the vicinity of ensheathing glia. To distinguish these GAL4$^+$ glia from astrocytes further, we used the GAT antibody (26) to mark astrocytes and found that the majority (~95%) of the GAL4$^+$ glia are negative for GAT (Fig. S1). In summary, *SPARC-GAL4*, *GRM56F03-GAL4*, and *GMR10E12-GAL4* mark ensheathing glia around the antennal lobe in the late pupal stage.

SPARC-GAL4 also drove reporter expression at 24 hAPF, enabling us to investigate the development of antennal lobe ensheathing glia. At 24 hAPF, before glomerular formation, ensheathing glia processes were restricted to the periphery of the antennal lobe (Fig. 1*A*). From 24–48 hAPF, axon terminals of ORNs invade the antennal lobe and target specific subregions to connect with their synaptic partners such as dendrites from PNs (17). We found that around 48 hAPF, when proto-glomeruli first emerged, ensheathing glia processes started to invade the antennal lobe from the lobe surface (Fig. 1*B*). Even at this initial stage of infiltration, ensheathing glia processes displayed a preference to grow along the borders between adjacent proto-glomeruli instead of growing into them (Fig. 1B_3). At 72 hAPF, as glomerular structures became more clearly separable, ensheathing glia processes had encircled most glomeruli (Fig. 1*C*). These processes remained on glomerular boundaries, with minimal extension into the glomeruli. Ensheathing glia wrapping of olfactory glomeruli was complete by the end of the pupal stage (Fig. 1*D*).

We also observed an increase in the number of *SPARC-GAL4*$^+$ ensheathing glia around the antennal lobe from 24–72 hAPF (Fig. 1*F*). This increase is caused, at least in part, by glial cell proliferation, because we could generate glia clones using mosaic analysis with a repressible cell marker (MARCM) (27) with heat shock-induced mitotic recombination at any point from 24–72 hAPF (see Fig. 3 and Fig. S3 below).

***Heartless* Knockdown in Ensheathing Glia Reduces Processes and Disrupts the Ensheathment Pattern.** To identify the molecular signals that control the extension of ensheathing glia processes, we tested ~50 candidate adhesion molecules, receptor kinases, and receptor phosphatases by RNAi and screened for potential defects in ensheathing glia development and antennal lobe organization. We found that expression of two independent RNAi targeting nonoverlapping regions of *heartless* (*htl*), an FGF receptor (28–30), caused a 70% reduction of ensheathing glia processes within the antennal lobe (Fig. 2 *A–D*). This phenotype is consistent with a previous discovery that FGF signaling is required for astrocytes to infiltrate the larval ventral nerve cord of *Drosophila* (26). However, the antennal lobe provides a unique opportunity to observe the response of neuronal compartmentalization to glia morphogenesis defects.

We found that many glomeruli became less clearly separable (arrowheads in Fig. 2 A_2, B_2, and C_2) when *htl* was knocked down. To quantify this effect, we used the relative SD (RSD) of the N-cadherin (Ncad) neuropil staining intensity as an index for the degree of compartmentalization, because incomplete antennal lobe compartmentalization would cause obscure glomerular borders and hence smaller variance in the neuropil staining signal. We found a significant reduction of RSD in *htl*-knockdown compared with wild-type antennal lobes (Fig. 2*E*). The remaining glomerular borders sometimes also lacked ensheathing glia processes that normally would divide the adjacent glomeruli (Fig. 2 *A–C*). We also observed ensheathing glia processes that extended within glomeruli; such extension into glomeruli is rarely observed in wild-type antennal lobes (Fig. 2B_1, arrowhead) and likely results from the poor establishment of glomerular borders. We quantified the localization pattern of the ensheathing glia processes relative to the glomerular compartments by plotting the intensity of the GFP signal derived from glial membranes together with the intensity of Ncad signal marking the neuropil (Fig. 2 A_3–C_3), and calculated their correlation coefficient (Fig. 2*F*). In control animals, Ncad and GFP signals exhibited strong anticorrelation (Fig. 2*F*), because ensheathing glia processes are preferentially located on the

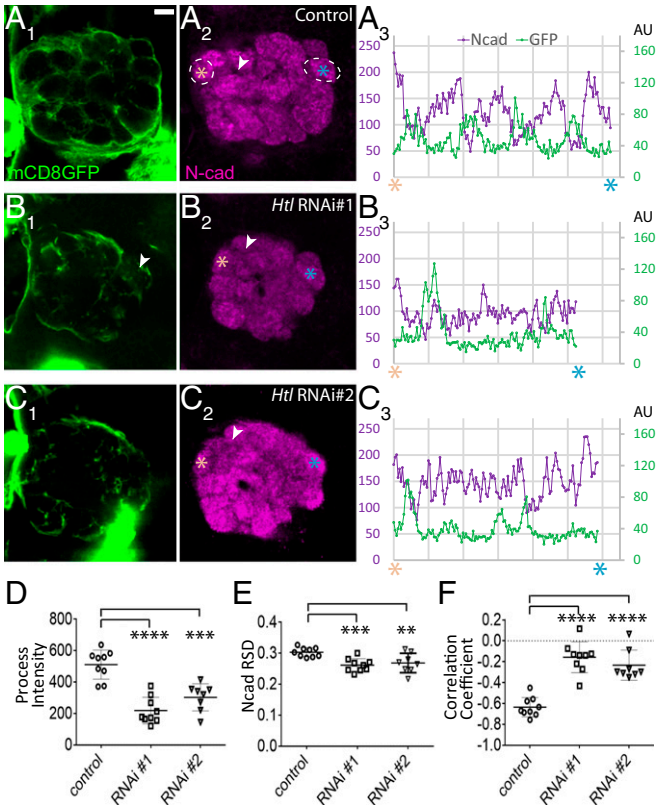

Fig. 2. Htl knockdown causes an altered ensheathing glia wrapping pattern and disrupts antennal lobe compartmentalization. (*A–C*) Confocal sections for the antennal lobe at 96 hAPF of wild type (*A*) and two different *UAS-Htl RNAi* constructs (RNAi#1: VDRC6692, RNAi#2: VDRC27180) driven by *SPARC-GAL4* (*B* and *C*). Ensheathing glia processes are labeled by *SPARC-GAL4* > *UAS-mCD8GFP*. Neuropil compartments are stained with Ncad antibody. GFP and Ncad intensities along a line between the center of DM6 and DA1 glomeruli (indicated by dashed circles in A_2 and by asterisks in A_2–C_2) are plotted in A_3–C_3, with the *x* axis indicating the position of each point on the line from DM6 to DA1 (*Left* to *Right*); fluorescence intensity was quantified in arbitrary units (AU). (*D*) Quantification of total GFP intensities normalized by antennal lobe size for wild-type and RNAi-expressing flies. (*E*) Quantification of the relative SD of Ncad intensities for each antennal lobe of wild-type and RNAi-expressing flies. (*F*) Correlation coefficient of GFP and Ncad intensities as plotted in A_3–C_3. (Scale bar: 10 μm.) Error bars represent SD. $^{**}P < 0.01$; $^{***}P < 0.001$, $^{****}P < 0.0001$. In this figure, subpanels represent the same sample in different imaging channels, unless otherwise specified.

borders of neuropil compartments instead of within the glomeruli. However, such anticorrelation was greatly diminished when *htl* was knocked down (Fig. 2*F*), suggesting that the loss of *htl* results in a disrupted ensheathment pattern.

***htl* Promotes Ensheathing Glia Survival and Cell-Autonomously Regulates Process Elaboration.** Htl is involved in cell differentiation, directional migration, and survival in a wide variety of tissues (26, 28, 31–34). Consistent with this involvement, we observed that *htl* knockdown caused a 40% reduction in the number of ensheathing glia near the antennal lobe as assayed by the LacZ nuclear marker (Fig. 3 *A–D*). This decrease is likely caused by cell death, because the expression of an apoptosis suppresser, P35 (35), in ensheathing glia largely rescued the reduction in cell number (Fig. S2); however, P35 expression did not rescue the reduction of ensheathing glia processes or the defect in glomerular compartmentalization (Fig. S2), suggesting that, in addition to its role in supporting glia survival, FGF signaling may regulate the morphogenesis of antennal lobe ensheathing glia.

To dissociate the role of *htl* in controlling glia survival and process extension, we used the MARCM technique (27) to generate single-cell clones of ensheathing glia homozygous for the $htl^{Ab42(null)}$ (30) allele in an otherwise heterozygous background. In this experiment, *GMR10E12-GAL4* was used to label the homozygous mutant cells. We used *UAS-mCD8GFP* to visualize glial processes (Fig. 3 *E* and *F*) and *UAS-nuclear-LacZ* (arrows in Fig. 3 E_1 and F_2) to visualize cell bodies of ensheathing glia in these MARCM clones. Compared with wild-type cells, the htl^{Ab42} single-cell clones exhibited a 50% reduction in the volume of glial processes (Fig. 3*G*) and a 50% reduction in total fluorescence intensity (Fig. S3). These reductions were accompanied by a decrease in the number of glomeruli that each ensheathing glia could access, as quantified by the number of glomerular borders to which each glia extended (Fig. 3*H*). Thus, this mosaic experiment demonstrated that *htl* is cell-autonomously required for process extension by ensheathing glia.

To determine the subcellular localization of the Htl protein, we used a fosmid transgenic line that produces Htl-GFP from an insertion that contains the extended genomic region covering *htl* (36) to analyze GFP signal within and around the antennal lobe during pupal development. At 24 hAPF, no Htl-GFP signal was detected inside the antennal lobe (Fig. 3*I*), consistent with the location of ensheathing glia processes (Fig. 1*A*). At 48 hAPF, we started to detect Htl-GFP signal between proto-glomeruli (Fig. 3*J*). By 72 hAPF, Htl-GFP signal was detected at most glomerular borders. [Also, a lower level of signal, which may originate from cell types other than ensheathing glia, such as astrocytes and potentially neurons, was detected within glomeruli (Fig. 3*K*).] The signal on glomerular borders coincided well with the wrapping pattern of the ensheathing glia over this developmental course (Fig. 1). These data support the hypothesis that Htl mediates FGF signaling to regulate the invasion of the antennal lobe and the wrapping of individual glomeruli by ensheathing glia.

Thisbe, an FGF Ligand, Is Required for the Wrapping of Glomeruli by Ensheathing Glia. We next assessed the identity and cellular source of FGF ligands that regulate ensheathing glia development. Htl responds to two FGF ligands, Thisbe (Ths) and Pyramus (Pyr) (37, 38). To test whether *ths* is required for the glia ensheathing the antennal lobe to form the wrapping pattern, we analyzed ensheathing glia and antennal lobe morphology in animals that carried different *ths* mutant alleles (39). The phenotypes we observed with loss of *htl* were all recapitulated in transheterozygous combinations of *ths* alleles [ths^{e02026}/ths^{759} and $Df(2R)ED2238/ths^{759}$]. There was an overall reduction of ensheathing glia processes and cell numbers in the antennal lobe of transheterozygous flies (Fig. 4 *A*, *B*, *E*, and *F*). Similar to the loss of *htl* from ensheathing glia, the antennal lobe of *ths* mutants showed defective compartmentalization as measured by reduced RSD values of Ncad staining (Fig. 4*G*) and a markedly reduced anticorrelation between the intensity of signal from ensheathing glia processes and the neuropil (Fig. 4*H*). These findings indicate that *ths* is required for ensheathing glia to wrap around glomeruli in the antennal lobe and that the failure to form a correct wrapping pattern could disrupt the compartmentalization of the antennal lobe neuropil.

Ths Is Produced by ORNs, PNs, and Antennal Lobe Local Interneurons. To identify which cell types express Ths, we took advantage of a MiMIC (Minos mediated integration cassette) insertion (23) located between two coding exons of the *ths* gene. We converted the MiMIC cassette to an artificial exon that contains the coding sequence for *2A-GAL4* (40). Thus, GAL4 can be produced along with the endogenous N terminus of Ths (encoded by the first two exons) and can drive reporter gene expression in the *ths* pattern. We then used this *Ths-GAL4* to express *UAS-mCD8GFP* to

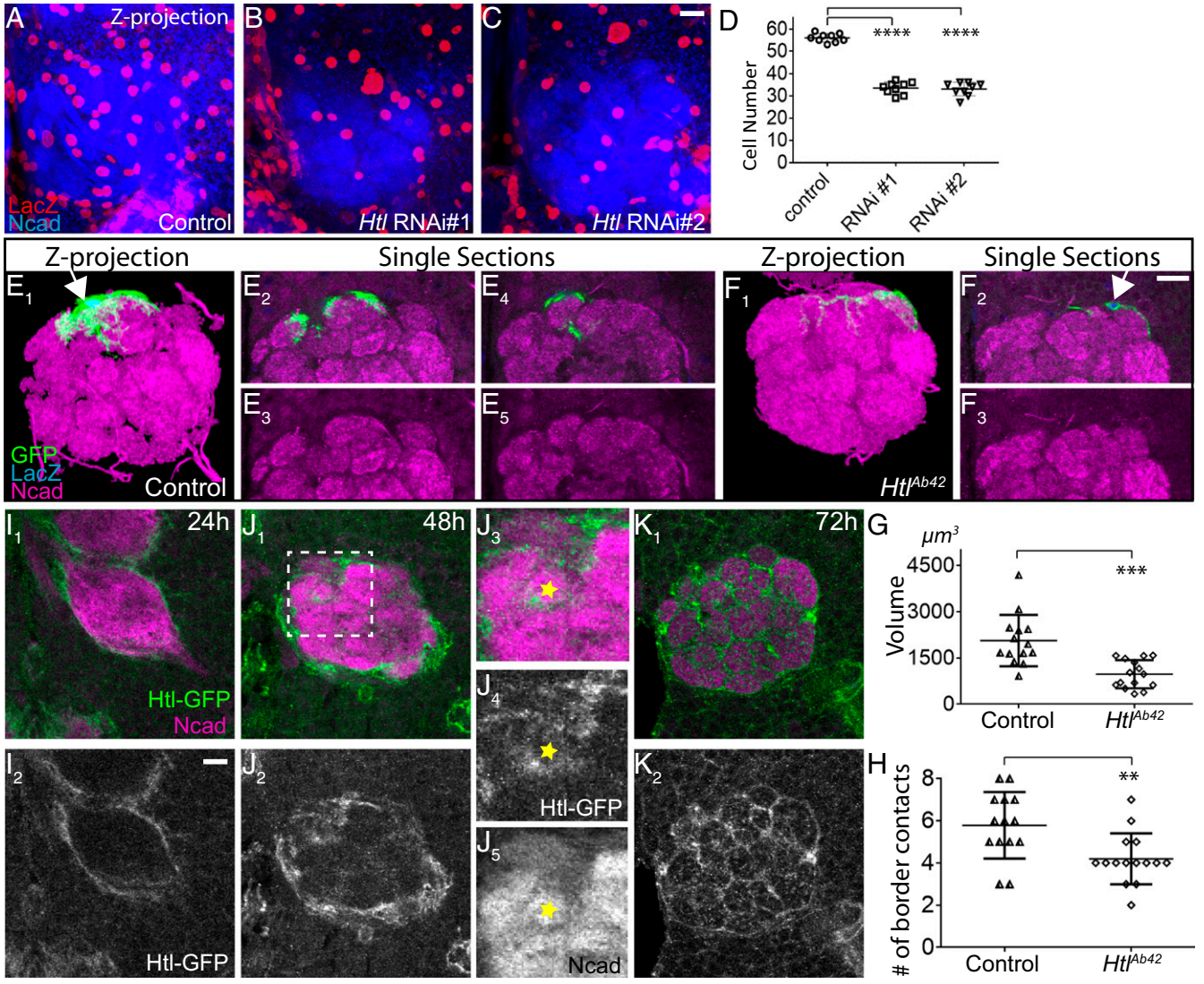

Fig. 3. Htl controls the number of ensheathing glia and cell-autonomously controls their morphology. (*A*–*C*) Projections of confocal sections along the *z* axis. Ensheathing glia cell bodies marked by *SPARC-GAL4* > *UAS-nuclear-LacZ* are shown in red, and Ncad antibody staining of the antennal lobe neuropil is shown in blue. (*D*) Quantification of the number of ensheathing glia cells in each antennal lobe. ****$P < 0.0001$. (*E* and *F*) Wild-type (*E*) and $htl^{Ab42/Ab42}$ (*F*) ensheathing glia single-cell MARCM clones in adult antennal lobe. Ensheathing glia processes labeled by *GMR10E12-GAL4* > *UAS-mCD8GFP* are shown in green; ensheathing glia nuclei marked by *UAS-nuclear-LacZ* are shown in blue; Ncad antibody staining for antennal lobe neuropil is shown in magenta. (*G*) Quantification of the volume of processes from each ensheathing glia labeled by MARCM. (*H*) Quantification of the number of borders contacted by each MARCM-labeled ensheathing glia. Error bars represent SD. **$P < 0.01$; ***$P < 0.001$. (*I*–*K*) Confocal sections of antennal lobe at 24 (*I*), 48 (*J*), and 72 (*K*) hAPF with Htl-GFP signal. The area of the dashed rectangle in J_1 is enlarged in J_3–J_5. The yellow stars mark the center of a proto-glomerulus around which ensheathing glia is wrapping. (Scale bars: 10 μm.) In this figure, subpanels represent the same sample in different imaging channels, unless otherwise specified.

visualize the cell bodies and projections of the Ths-producing cells. In the antennal lobe, neuronal processes from PNs, ORNs, and local interneurons (LNs) are all labeled, suggesting that all three major neuronal types produce Ths (Fig. 4*I*).

To determine the contributions of each of these cell types, we used an intersectional strategy in which *Ths-GAL4* was combined with Flp recombinases that are specifically expressed in ORNs (*ey-FLP*) (41) or PNs (*GH146-FLP*) (42). With a FLP-out reporter, *UAS-FRT-stop-FRT-mCD8GFP* (42), we found a number of ORN and PN classes were *Ths-GAL4*$^+$ based on glomerular labeling (Fig. 4 *J* and *K*). At least 45 cell bodies over all sections of the antennal lobe were *Ths-GAL4*$^+$ without intersection (Fig. 4*I*); however, only 19 of them (constituting the majority of PNs innervating ∼40 glomeruli) were *GH146-Flp*$^+$ PNs; this finding is consistent with the small number of glomeruli (approximately seven) labeled by the intersection of *GH146-Flp* and *Ths-GAL4* (Fig. 4*K*). This difference is likely caused by the contribution from LNs, whose cell bodies are also located around the antennal lobe (43, 44), whereas ORN cell bodies are located in the peripheral sensory organs.

We used two approaches to validate the notion that LNs produce Ths. First, we suppressed the expression from most PNs by combining *GH146-GAL80* (42) together with *Ths-GAL4*. After PN-derived signal was largely eliminated, ∼27 cell bodies remained around the antennal lobe. The projection pattern of these neurons covered the entire antennal lobe (Fig. 4*L*), as is characteristic of the majority of LNs (43). Second, we used *Ths-GAL4* to label single cells by the MARCM technique and were able to identify MARCM clones for LNs (Fig. 4*M*). In summary, Ths is produced by a subset of ORNs, PNs, and LNs.

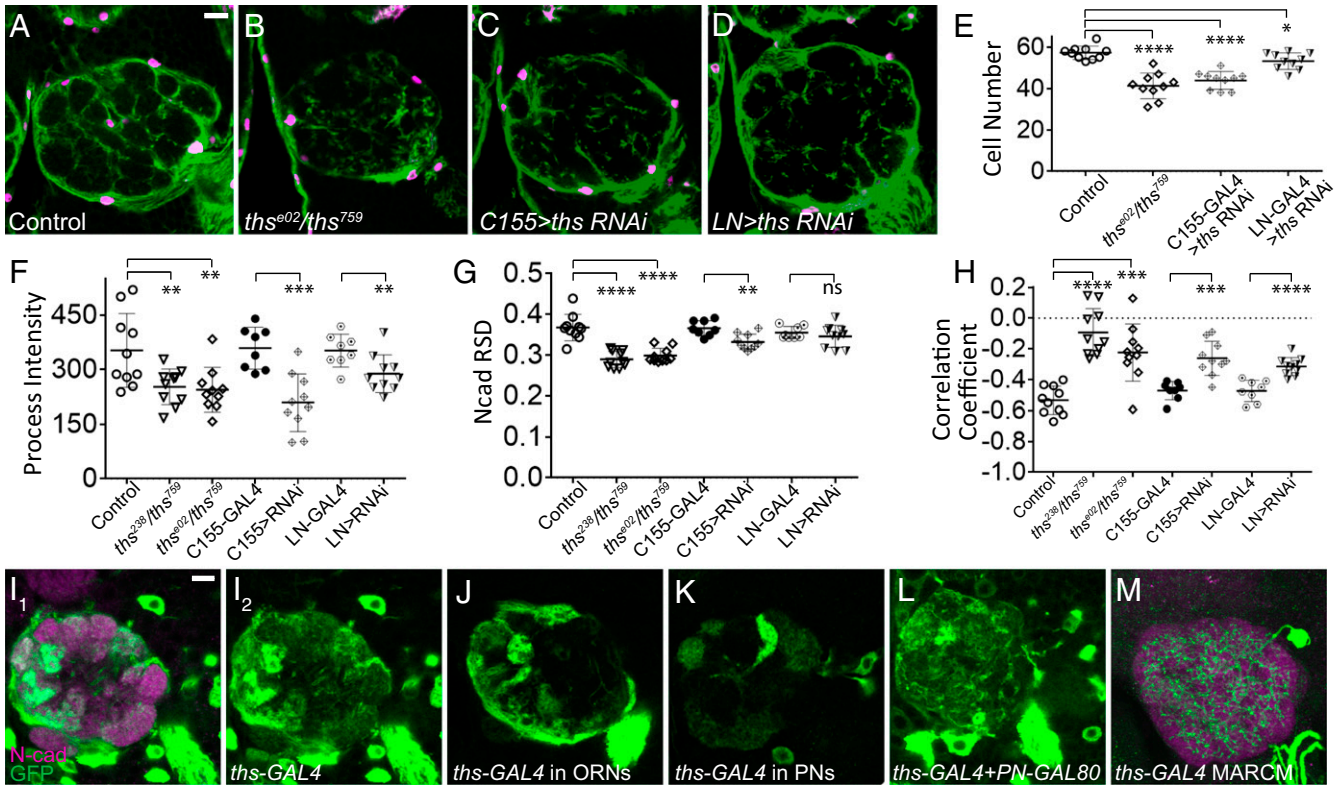

Fig. 4. *Ths* is expressed in olfactory neurons and is required for ensheathing glia to wrap glomeruli. (*A–D*) Ensheathing glia wrapping pattern in the wild type (*A*), *ths* mutant (ths^{e02} denotes the ths^{e02026} allele) (*B*), pan-neural *C155-GAL4*– (*C*), and LN $orb^{0449\text{-}GAL4}$– (*D*) driven RNAi against *ths*. Ensheathing glia processes labeled by *SPARC-QF* > *QUAS-mtdT* are shown in green. Ensheathing glia nuclei marked with *QUAS-nuclear-LacZ* are shown in magenta. (*E–H*) Quantification of the number of ensheathing glia (*E*), process intensity (*F*), relative SD of Ncad staining (*G*), and the correlation coefficient for the intensities of ensheathing glia process and neuropil staining (*H*). Error bars represent SD. *$P < 0.05$; **$P < 0.01$; ***$P < 0.001$; ****$P < 0.0001$; ns (not significant), $P > 0.05$. (*I*) The pattern of *ths* expression revealed by *ths-GAL4* > *UAS-mCD8GFP* (green). Magenta in I_1 shows Ncad counterstaining. (*J*) *ey-FLP* intersects with *ths-GAL4* together with *UAS-FRT-stop-FRT-mCD8GFP* to show the pattern of *ths* expression in ORNs. (*K*) The *GH146-FLP* intersection shows the pattern of *ths* expression in PNs. (*L*) *ths-GAL4*$^+$ LN cell bodies and LN and ORN processes after *GH146-GAL80* suppression of *ths-GAL4* in most PNs. (*M*) MARCM labels a single LN that is positive for *ths-GAL4*. GFP, green; Ncad, magenta. All images are confocal sections of adult antennal lobes except *M*, which is a projection of Z stacks. (Scale bars: 10 μm.) In this figure, subpanels represent the same sample in different imaging channels, unless otherwise specified.

LN-Derived Ths Is Necessary for Ensheathing Glia Wrapping. To test in which cell type(s) Ths functions to regulate ensheathing glia morphogenesis and antennal lobe compartmentalization, we used RNAi to knock down *ths* in ORNs (*Pebbled-GAL4*), PNs (*GH146-GAL4*), LNs, and all neurons (*C155-GAL4*), respectively, while labeling the ensheathing glia by *SPARC-QF*, which we converted from *SPARC-GAL4* (23). Pan-neuronal knockdown of *ths* recapitulated the phenotypes observed in *ths* mutants (Fig. 4 *C* and *E–H*). Knocking down *ths* specifically in LNs by $orb^{0449\text{-}GAL4}$ (Fig. S4), a GAL4 line identified from the InSite screen (45), resulted in a mild but significant defect in ensheathing glia wrapping and antennal lobe glomerulus integrity (Fig. 4 *D* and *E–H*). Knocking down *ths* in PNs did not cause significant defects (Fig. S5). We also used MARCM combined with a cell-lethal strategy (41) to create a near pan-ORN mutant background for *ths* and did not find defects in ensheathing glia wrapping (Fig. S5). Possible explanations for the milder phenotypes in LN knockdown compared with pan-neuronal knockdown are (*i*) pan-neuronal GAL4 may have stronger and/or earlier expression than the LN-GAL4 and therefore causes more effective knockdown; (*ii*) LN-GAL4 does not include all LNs; or (*iii*) Ths from ORNs and PNs synergize with Ths from LNs. In any case, our data indicate that LN is an essential cellular source of Ths in the antennal lobe for directing ensheathing glia wrapping.

Ths Can Instruct Glomerular Wrapping with a High Spatial Specificity. We have shown that FGF signaling is necessary for ensheathing glia to extend processes into the antennal lobe and demarcate individual glomeruli. To test whether FGF signaling can instruct ensheathing glia to wrap around selected neuropil compartments, we expressed *ths* in only one class of ORNs (VA1v) using a GAL4 under the control of the promoter of the odorant receptor specifically expressed in this class (*Or47b-GAL4*). We observed that overexpression resulted in hyperwrapping of the VA1v glomerulus by ensheathing glia (Fig. 5 *B* and *D*). This effect was highly localized, because, in addition to VA1v, only the adjacent VA1d glomerulus was slightly hyperwrapped (Fig. 5*D*), likely because of the intensified ensheathing glia processes on its border shared with VA1v. Hyperwrapping did not extend to the DA1 glomerulus (Fig. 5*D*), which is one glomerulus away from the VA1v glomerulus. There also was an excess of glia cells around the hyperwrapped VA1v glomerulus (Fig. 5*F*).

Similarly, overexpressing Ths in *Mz19-GAL4*$^+$ PNs, which send dendrites to DA1 and VA1d, caused local hyperwrapping of these glomeruli, as well as a local increase in ensheathing glia cells (Fig. 5 *C*, *E*, and *G*). We have consistently noticed that *Mz19-GAL4* activity is stronger in DA1 PNs than in VA1d PNs (46). Accordingly, glial hyperwrapping was more pronounced around DA1 than around VA1d. These results suggest that Ths acts locally as a spatial cue to instruct ensheathing glia to infiltrate the antennal lobe.

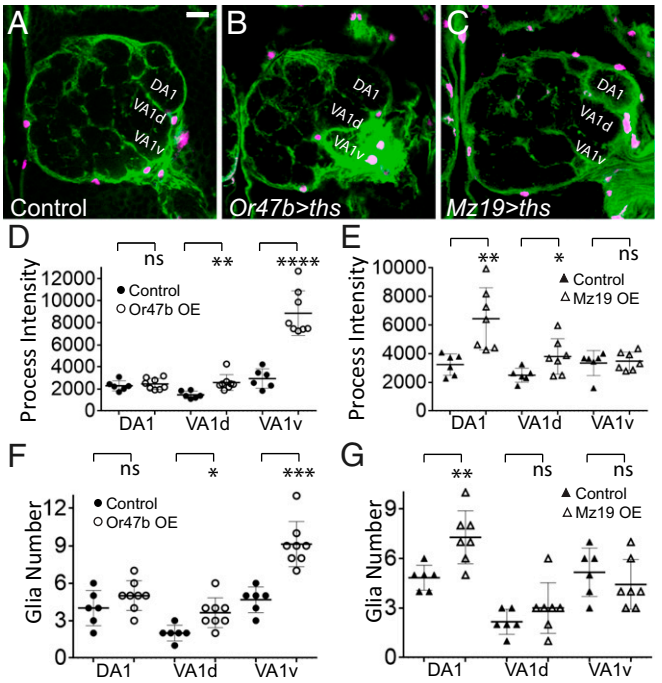

Fig. 5. Changes in ensheathing glia processes and numbers in response to local overexpression of *ths*. (*A*–*C*) Confocal sections of adult antennal lobe of the wild type (*A*) or overexpression of *UAS-ths* by *Or47b-GAL4* (*B*) or by *Mz19-GAL4* (*C*). *SPARC-QF* > *QUAS-mtdT* labels ensheathing glia processes are shown in green; ensheathing glia nuclei marked with *QUAS-nuclear-LacZ* are shown in magenta. (Scale bar: 10 μm.) (*D* and *E*) Quantification of signal intensities of ensheathing glia processes around each glomerulus normalized by the perimeter of the corresponding glomerulus. (*F* and *G*) Quantification of ensheathing glia numbers within 5 μm of the surface of each glomerulus. Error bars represent SD. **P* < 0.05; ***P* < 0.01; ****P* < 0.001; *****P* < 0.0001; ns (not significant), *P* > 0.05.

FGF Signaling Ensures Accurate Neuronal Targeting. Last, we examined whether glia-wrapping defects could disrupt neuronal projections to the glomerular compartments. We used membrane proteins under the control of specific odorant receptor promoters (*Or88a-mtdT* and *Or47b-rCD2*) to label two ORN classes that project their axons to two adjacent glomeruli, VA1v and VA1d (Fig. 6*A*). When *ths* was knocked down with a pan-neuronal driver, *C155-GAL4*, VA1v and VA1d ORN axons still reached their target area in the ventrolateral antennal lobe. However, they failed to establish exclusive territories for their axonal arborization and instead had partially overlapping axonal terminals (Fig. 6*B*). Likewise, in *ths*-mutant animals, VA1v and VA1d axon terminals partially intermingled, rather than remaining confined to their respective glomerular compartments (Fig. 6*C*; quantified in Fig. 6*D*). Thus, FGF signaling between neurons and ensheathing glia is essential for antennal lobe compartmentalization and for the targeting accuracy of ORN axons.

Discussion

The use of discrete neuropil compartments for organizing and signaling information is widespread in invertebrate and vertebrate nervous systems. In both the fly antennal lobe and vertebrate olfactory bulb, axons from different ORN classes are segregated into distinct glomeruli (47). The rodent barrel cortex also uses discrete compartments, the barrels, to represent individual whiskers (48). In this study, we show that FGF signaling between neurons and glia mediates neural compartment formation in the *Drosophila* antennal lobe.

Members of the FGF family have diverse functions in a variety of tissues in both vertebrates and invertebrates (49, 50). Vertebrate FGFs regulate not only neural proliferation, differentiation, axon guidance, and synaptogenesis but also gliogenesis, glial migration, and morphogenesis (51–55). Many of these roles are conserved in invertebrates. For example, Ths and Pyr induce glial wrapping of axonal tracts (32, 33), much like the role other FGF members play in regulating myelin sheaths in mammals (55). Ths and Pyr also control *Drosophila* astrocyte migration and morphogenesis (26); likewise, FGF signaling promotes the morphogenesis of mammalian astrocytes (56). Therefore, studying the signaling pathways in *Drosophila* will extend our understanding of the principles of neural development.

In ensheathing glia, whose developmental time course and mechanisms have not been well documented before this study, we observed a glial response to FGF signaling reminiscent of the paradigm shown previously (26, 32, 57); however, the exquisite compartmental structure of the *Drosophila* antennal lobe and genetic access allowed us to scrutinize further the changes of neuropil structure and projection patterns that occurred alongside morphological phenotypes in ensheathing glia. We demonstrated the requirement for Ths in LNs, although it is possible that ORNs and PNs also contribute. We also tested the function of the other ligand, Pyr, in antennal lobe development. We did not detect any change in ensheathing glia morphology with *pyr* RNAi, and double

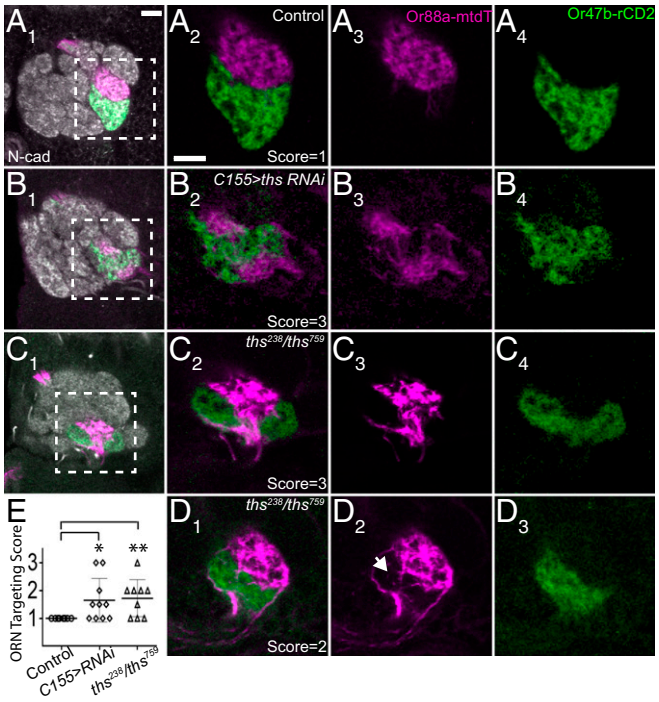

Fig. 6. Loss of *ths* results in defects in olfactory receptor neuron targeting. (*A*–*D*) Confocal sections of the adult antennal lobe, with *Or88a-mtdT* and *Or47b-rCD2* labeling ORN axons that target VA1d (magenta) and VA1v (green) glomeruli, respectively. Images within the dashed rectangles in the far left column are enlarged in columns 2–4. (*A*) Wild type. (*B*) *C155-GAL4*–driven *ths* RNAi. (*C* and *D*) *ths* mutant flies showed severe intermingling of VA1d and VA1v ORN terminals (*C*) and a mild spillover of VA1d ORN axons (*D*, arrow). ths^{238} denotes the *Df(2R)ED2238* allele. (Scale bar: 10 μm.) (*E*) Quantification of the accuracy of ORN axon targeting: 1, normal; 2, mild spillover; 3, severe intermingling. Each symbol represents one fly with two antennal lobes scored separately and averaged. Error bars represent SD. **P* < 0.05; ***P* < 0.01. In this figure, subpanels represent the same sample in different imaging channels, unless otherwise specified.

RNAi against *ths* and *pyr* did not enhance the phenotype compared with *ths* knockdown alone.

FGF signaling in glomerular wrapping appears to be highly local. In our overexpression experiments, the hyperwrapping effect was restricted to the glomerulus where the ligand is excessively produced and did not spread to nearby nonadjacent glomeruli. These experiments suggest that Ths communicates locally to instruct glial ensheathment of the glomeruli rather than diffusing across several microns to affect nearby glomeruli. Because heparan sulfate proteoglycans are known to act as FGF coreceptors by modulating the activity and spatial distribution of the ligands (50, 58, 59), we speculate that Ths in the antennal lobe may be subject to such regulation to limit its diffusion and long-range effect.

Our data showed that deficient ensheathment of antennal lobe glomeruli is accompanied by imprecise ORN axon targeting. However, we cannot determine whether these targeting defects reflect initial axon-targeting errors or a failure to stabilize or maintain the discrete targeting pattern. Previous models for the establishment of antennal lobe wiring specificity suggested that the glomerular map is discernable by the time glia processes start to infiltrate the antennal lobe (17). Because of a lack of class-specific ORN markers for early developmental stages, the relative timing between when neighboring ORN classes refine their axonal targeting to discrete compartments and when ensheathing glia barriers are set up still remains unclear. Nevertheless, our discovery that FGF signaling functions in the formation of discrete neuronal compartments in the antennal lobe highlights an essential role for glia in the precise assembly of neural circuits.

Methods

Immunostaining. Tissue dissection and immunostaining were performed according to previously described methods (60). Primary antibodies used in this study include rat anti-DNcad [DN-Ex #8; 1:40; Developmental Studies Hybridoma Bank (DSHB)], chicken anti-GFP (1:1,000; Aves Labs), rabbit anti-DsRed (1:500; Clontech), mouse anti-rCD2 (OX-34; 1:200; AbD Serotec), rat anti-HA (1 μg/mL; Roche), mouse nc82 (1:35; DSHB), mouse anti-Repo (1:50; DSHB), rabbit anti–β-Galactosidase (1:125; MP Biomedicals), rabbit anti-GAT (1:3,000; a gift from Marc Freeman, Vollum Institute, Oregon Health and Science University, Portland, OR), and mouse anti–β-Galactosidase (1:1,000; Promega). Secondary antibodies were raised in goat or donkey against rabbit, mouse, rat, and chicken antisera (Jackson ImmunoResearch) conjugated to Alexa 405, FITC, 568, or 647. Confocal images were collected with a Zeiss LSM 780 laser scanning microscope and were processed with Zen (Zeiss), ImageJ (NIH), and Imaris (Bitplane) software.

Mosaic Analysis. The hsFlp MARCM analyses were performed as previously described (27, 61) with slight modifications. *GMR10E12-GAL4* was used for labeling ensheathing glia in adult-stage *Drosophila*. Flies were kept at 18 °C and were heat shocked for 30 min at 37 °C between 0 and 24 hAPF.

Data Analysis. Confocal sections of antennal lobes (Figs. 2 and 4) were analyzed by ImageJ software to measure integrated intensity value, area size, mean, and SD for the region of interest (ROI) manually selected based on Ncad counterstaining. Process intensity was calculated using the integrated intensity value of the antennal lobe section crossing the DA1 and DM6 glomeruli normalized by the area size of the antennal lobe of that section. The Plot Profile function in ImageJ was used to measure signal intensities for ensheathing glia processes and Ncad along the selected lines. Glia cell number was counted manually based on LacZ staining within 10 μm of the surface of the antennal lobe determined by Ncad counterstaining. To quantify the MARCM clones (Fig. 3), confocal sections of marked ensheathing glia were processed by Imaris software by manually thresholding the images by a set of consistent parameters, followed by automatic measurement of the volume and total intensity of glia processes. In the overexpression experiment (Fig. 5), the ROI was selected manually by including the inner region and the boundaries of the glomerulus of interest based on Ncad counterstaining. Process intensity was defined as the integrated intensity value divided by the perimeter of the ROI selection. The glia number was counted manually based on LacZ signal within 5 μm of the surface of each glomerulus. ORN targeting defects (Fig. 6) were scored by an experimenter blind to the genotype. Graphs were generated using the GraphPad Prism software; mean ± SD were shown on the graphs. Statistical significance was calculated with GraphPad Prism using a two-tailed Student's *t* test (Figs. 2–5) or a Mann–Whitney *U* test for the nonparametric data in Fig. 6.

ACKNOWLEDGMENTS. We thank M. Freeman, C. Klämbt, H. Bellen, T. Clandinin, and the Vienna and Bloomington Stock Centers for reagents and X. Wang, J. Lui, A. Shuster, J. Ren, H. Li, T. Li, and L. DeNardo for discussion and helpful comments on the manuscript. This work was supported by NIH Grant R01 DC005982 (to L.L.). L.L. is a Howard Hughes Medical Institute investigator.

1. Mitchell KJ, et al. (1996) Genetic analysis of Netrin genes in *Drosophila*: Netrins guide CNS commissural axons and peripheral motor axons. *Neuron* 17:203–215.
2. Kidd T, Bland KS, Goodman CS (1999) Slit is the midline repellent for the robo receptor in *Drosophila*. *Cell* 96:785–794.
3. Michailov GV, et al. (2004) Axonal neuregulin-1 regulates myelin sheath thickness. *Science* 304:700–703.
4. Pfrieger FW, Barres BA (1997) Synaptic efficacy enhanced by glial cells in vitro. *Science* 277:1684–1687.
5. Ullian EM, Sapperstein SK, Christopherson KS, Barres BA (2001) Control of synapse number by glia. *Science* 291:657–661.
6. Mauch DH, et al. (2001) CNS synaptogenesis promoted by glia-derived cholesterol. *Science* 294:1354–1357.
7. Christopherson KS, et al. (2005) Thrombospondins are astrocyte-secreted proteins that promote CNS synaptogenesis. *Cell* 120:421–433.
8. Paolicelli RC, et al. (2011) Synaptic pruning by microglia is necessary for normal brain development. *Science* 333:1456–1458.
9. Schafer DP, et al. (2012) Microglia sculpt postnatal neural circuits in an activity and complement-dependent manner. *Neuron* 74:691–705.
10. Bezzi P, et al. (1998) Prostaglandins stimulate calcium-dependent glutamate release in astrocytes. *Nature* 391:281–285.
11. Araque A, Parpura V, Sanzgiri RP, Haydon PG (1998) Glutamate-dependent astrocyte modulation of synaptic transmission between cultured hippocampal neurons. *Eur J Neurosci* 10:2129–2142.
12. Araque A, Sanzgiri RP, Parpura V, Haydon PG (1998) Calcium elevation in astrocytes causes an NMDA receptor-dependent increase in the frequency of miniature synaptic currents in cultured hippocampal neurons. *J Neurosci* 18:6822–6829.
13. Araque A, et al. (2014) Gliotransmitters travel in time and space. *Neuron* 81:728–739.
14. Stork T, Bernardos R, Freeman MR (2012) Analysis of glial cell development and function in *Drosophila*. *Cold Spring Harb Protoc* 2012:1–17.
15. Awasaki T, Lai SL, Ito K, Lee T (2008) Organization and postembryonic development of glial cells in the adult central brain of *Drosophila*. *J Neurosci* 28:13742–13753.
16. Jhaveri D, Sen A, Rodrigues V (2000) Mechanisms underlying olfactory neuronal connectivity in *Drosophila*-the atonal lineage organizes the periphery while sensory neurons and glia pattern the olfactory lobe. *Dev Biol* 226:73–87.
17. Jefferis GS, et al. (2004) Developmental origin of wiring specificity in the olfactory system of *Drosophila*. *Development* 131:117–130.
18. Vosshall LB, Wong AM, Axel R (2000) An olfactory sensory map in the fly brain. *Cell* 102:147–159.
19. Gao Q, Yuan B, Chess A (2000) Convergent projections of *Drosophila* olfactory neurons to specific glomeruli in the antennal lobe. *Nat Neurosci* 3:780–785.
20. Doherty J, Logan MA, Taşdemir OE, Freeman MR (2009) Ensheathing glia function as phagocytes in the adult *Drosophila* brain. *J Neurosci* 29:4768–4781.
21. Kazama H, Yaksi E, Wilson RI (2011) Cell death triggers olfactory circuit plasticity via glial signaling in *Drosophila*. *J Neurosci* 31:7619–7630.
22. Jenett A, et al. (2012) A GAL4-driver line resource for *Drosophila* neurobiology. *Cell Rep* 2:991–1001.
23. Venken KJ, et al. (2011) MiMIC: A highly versatile transposon insertion resource for engineering *Drosophila* melanogaster genes. *Nat Methods* 8:737–743.
24. Kremer MC, Jung C, Batelli S, Rubin GM, Gaul U (2017) The glia of the adult *Drosophila* nervous system. *Glia* 65:606–638.
25. Halter DA, et al. (1995) The homeobox gene repo is required for the differentiation and maintenance of glia function in the embryonic nervous system of *Drosophila* melanogaster. *Development* 121:317–332.
26. Stork T, Sheehan A, Tasdemir-Yilmaz OE, Freeman MR (2014) Neuron-glia interactions through the Heartless FGF receptor signaling pathway mediate morphogenesis of *Drosophila* astrocytes. *Neuron* 83:388–403.
27. Lee T, Luo L (1999) Mosaic analysis with a repressible cell marker for studies of gene function in neuronal morphogenesis. *Neuron* 22:451–461.
28. Beiman M, Shilo BZ, Volk T (1996) Heartless, a *Drosophila* FGF receptor homolog, is essential for cell migration and establishment of several mesodermal lineages. *Genes Dev* 10:2993–3002.
29. Shishido E, Higashijima S, Emori Y, Saigo K (1993) Two FGF-receptor homologues of *Drosophila*: One is expressed in mesodermal primordium in early embryos. *Development* 117:751–761.
30. Gisselbrecht S, Skeath JB, Doe CQ, Michelson AM (1996) Heartless encodes a fibroblast growth factor receptor (DFR1/DFGF-R2) involved in the directional migration of early mesodermal cells in the *Drosophila* embryo. *Genes Dev* 10:3003–3017.

31. Michelson AM, Gisselbrecht S, Zhou Y, Baek KH, Buff EM (1998) Dual functions of the heartless fibroblast growth factor receptor in development of the *Drosophila* embryonic mesoderm. *Dev Genet* 22:212–229.
32. Franzdóttir SR, et al. (2009) Switch in FGF signalling initiates glial differentiation in the *Drosophila* eye. *Nature* 460:758–761.
33. Shishido E, Ono N, Kojima T, Saigo K (1997) Requirements of DFR1/Heartless, a mesoderm-specific *Drosophila* FGF-receptor, for the formation of heart, visceral and somatic muscles, and ensheathing of longitudinal axon tracts in CNS. *Development* 124:2119–2128.
34. Mandal L, Banerjee U, Hartenstein V (2004) Evidence for a fruit fly hemangioblast and similarities between lymph-gland hematopoiesis in fruit fly and mammal aorta-gonadal-mesonephros mesoderm. *Nat Genet* 36:1019–1023.
35. Hay BA, Wolff T, Rubin GM (1994) Expression of baculovirus P35 prevents cell death in *Drosophila*. *Development* 120:2121–2129.
36. Sarov M, et al. (2016) A genome-wide resource for the analysis of protein localisation in *Drosophila*. *Elife* 5:e12068.
37. Stathopoulos A, Tam B, Ronshaugen M, Frasch M, Levine M (2004) Pyramus and Thisbe: FGF genes that pattern the mesoderm of *Drosophila* embryos. *Genes Dev* 18:687–699.
38. Gryzik T, Müller HA (2004) FGF8-like1 and FGF8-like2 encode putative ligands of the FGF receptor Htl and are required for mesoderm migration in the *Drosophila* gastrula. *Curr Biol* 14:659–667.
39. Klingseisen A, Clark IB, Gryzik T, Müller HA (2009) Differential and overlapping functions of two closely related *Drosophila* FGF8-like growth factors in mesoderm development. *Development* 136:2393–2402.
40. Diao F, et al. (2015) Plug-and-play genetic access to *Drosophila* cell types using exchangeable exon cassettes. *Cell Rep* 10:1410–1421.
41. Newsome TP, Asling B, Dickson BJ (2000) Analysis of *Drosophila* photoreceptor axon guidance in eye-specific mosaics. *Development* 127:851–860.
42. Hong W, et al. (2009) Leucine-rich repeat transmembrane proteins instruct discrete dendrite targeting in an olfactory map. *Nat Neurosci* 12:1542–1550.
43. Chou YH, et al. (2010) Diversity and wiring variability of olfactory local interneurons in the *Drosophila* antennal lobe. *Nat Neurosci* 13:439–449.
44. Stocker RF, Lienhard MC, Borst A, Fischbach KF (1990) Neuronal architecture of the antennal lobe in *Drosophila* melanogaster. *Cell Tissue Res* 262:9–34.
45. Gohl DM, et al. (2011) A versatile in vivo system for directed dissection of gene expression patterns. *Nat Methods* 8:231–237.
46. Hong W, Mosca TJ, Luo L (2012) Teneurins instruct synaptic partner matching in an olfactory map. *Nature* 484:201–207.
47. Komiyama T, Luo L (2006) Development of wiring specificity in the olfactory system. *Curr Opin Neurobiol* 16:67–73.
48. Woolsey TA, Van der Loos H (1970) The structural organization of layer IV in the somatosensory region (SI) of mouse cerebral cortex. The description of a cortical field composed of discrete cytoarchitectonic units. *Brain Res* 17:205–242.
49. Ornitz DM, Itoh N (2015) The fibroblast growth factor signaling pathway. *Wiley Interdiscip Rev Dev Biol* 4:215–266.
50. Muha V, Müller HA (2013) Functions and mechanisms of fibroblast growth factor (FGF) signalling in *Drosophila melanogaster*. *Int J Mol Sci* 14:5920–5937.
51. Guillemot F, Zimmer C (2011) From cradle to grave: The multiple roles of fibroblast growth factors in neural development. *Neuron* 71:574–588.
52. Smith KM, et al. (2006) Midline radial glia translocation and corpus callosum formation require FGF signaling. *Nat Neurosci* 9:787–797.
53. Perraud F, Labourdette G, Miehe M, Loret C, Sensenbrenner M (1988) Comparison of the morphological effects of acidic and basic fibroblast growth factors on rat astroblasts in culture. *J Neurosci Res* 20:1–11.
54. Reilly JF, Maher PA, Kumari VG (1998) Regulation of astrocyte GFAP expression by TGF-beta1 and FGF-2. *Glia* 22:202–210.
55. Furusho M, Dupree JL, Nave KA, Bansal R (2012) Fibroblast growth factor receptor signaling in oligodendrocytes regulates myelin sheath thickness. *J Neurosci* 32: 6631–6641.
56. Kang K, Lee SW, Han JE, Choi JW, Song MR (2014) The complex morphology of reactive astrocytes controlled by fibroblast growth factor signaling. *Glia* 62:1328–1344.
57. Gibson NJ, Tolbert LP, Oland LA (2012) Activation of glial FGFRs is essential in glial migration, proliferation, and survival and in glia-neuron signaling during olfactory system development. *PLoS One* 7:e33828.
58. Shimokawa K, et al. (2011) Cell surface heparan sulfate chains regulate local reception of FGF signaling in the mouse embryo. *Dev Cell* 21:257–272.
59. Baeg GH, Perrimon N (2000) Functional binding of secreted molecules to heparan sulfate proteoglycans in *Drosophila*. *Curr Opin Cell Biol* 12:575–580.
60. Sweeney LB, et al. (2007) Temporal target restriction of olfactory receptor neurons by semaphorin-1a/plexinA-mediated axon-axon interactions. *Neuron* 53:185–200.
61. Komiyama T, Carlson JR, Luo L (2004) Olfactory receptor neuron axon targeting: Intrinsic transcriptional control and hierarchical interactions. *Nat Neurosci* 7:819–825.